Regenerative Therapy 25 (2024) 320–330

Contents lists available at ScienceDirect

Regenerative Therapy

journal homepage: http://www.elsevier.com/locate/reth

Original Article

Extracellular vesicles derived from HuMSCs alleviate daunorubicin-induced cardiac microvascular injury via miR-186-5p/PARP9/STAT1 signal pathway

Shule Zhang [a], Dong Li [b], Linghong Liu [b], Qing Shi [b], Xiuli Ju [a, b, *]

[a] Department of Pediatrics, Qilu Hospital of Shandong University, Jinan 250012, China
[b] Cryomedicine Laboratory, Qilu Hospital of Shandong University, Jinan 250012, China

ARTICLE INFO

Article history:
Received 10 November 2023
Received in revised form
21 January 2024
Accepted 25 January 2024

Keywords:
Daunorubicin-induced cardiac injury
Endothelial damage
Mesenchymal stem cell
Extracellular vesicles
microRNA
PARP9

ABSTRACT

Introduction: It is essential to acknowledge that the cardiovascular toxicity associated with anthracycline drugs can be partially attributed to the damage inflicted on blood vessels and endothelial cells. Extracellular vesicles (EVs) derived from mesenchymal stem cells (MSCs) have the potential to repair cellular processes and promote tissue regeneration through the transfer of signaling molecules such as miRNAs. In the present study, we investigated the effects of MSC-EVs on daunorubicin (DNR)-damaged human cardiac microvascular endothelial cells (HCMEC) and developing blood vessels of Chicken Chorioallantoic Membrane (CAM) in vivo.

Materials and methods: We constructed in vitro and in vivo models of DNR-damaged endothelial cells and developing blood vessel. Scratch wound assays, EdU assays, tube formation assays, and SA-β-Gal staining were used to evaluate the effects of MSC-EVs on cell migration, proliferation, angiogenesis capacity and cell senescence. Blood vessel area was used to assess the effects of MSC-EVs on CAM vasculature. RT-qPCR was used to detect the mRNA expression levels of inflammatory molecules. RNA sequencing was employed to compare differential gene expression and downstream regulatory mechanisms. RNA interference experiments and miRNA mimic overexpression experiments were used to validate the regulatory effects of target genes and downstream signaling pathways.

Results: We found that MSC-EVs improved the migration, proliferation, and angiogenesis of HCMEC, while also alleviating cellular senescence. The angiogenic effect on the developing blood vessels was confirmed in vivo. We identified that MSC-EVs downregulated the expression of PARP9, thereby inhibiting the STAT1/pSTAT1 signaling pathway. This downregulation effect is likely mediated by the transfer of miR-186-5p from MSC-EVs to HCMEC. Overexpression of miR-186-5p in DNR-damaged HCMEC also exhibited the aforementioned downregulation effect. In vivo, the introduction of miR-186-5p mimics enhanced angiogenesis in the CAM model.

Conclusions: To summarize, our study reveals that MSC-EVs can restore the cellular function of DNR-damaged HCMEC and alleviate cellular senescence through the miR-185-5p-PARP9-STAT1/pSTAT1 pathway. This finding highlights the potential of MSC-EVs as a therapeutic strategy for mitigating the detrimental effects of anthracycline-induced endothelial damage.

Abbreviations: DNR, Daunorubicin; MSC-EVs, Extracellular vesicles (EVs) derived from mesenchymal stem cells; HCMEC, human cardiac microvascular endothelial cells; CAM, Chicken Chorioallantoic Membrane; IFN-I, type I interferon; PARP9, poly (ADP-ribose) polymerase family member 9.

* Corresponding author. Department of Pediatrics, Qilu Hospital of Shandong University, 107 Wenhua Xilu, Jinan, 250012, Shandong, China.
E-mail address: jxlqlyy@163.com (X. Ju).

Peer review under responsibility of the Japanese Society for Regenerative Medicine.

https://doi.org/10.1016/j.reth.2024.01.011

1. Introduction

Daunorubicin (DNR), an anthracycline chemotherapy drug, is commonly used as a primary medication in first-line treatment for pediatric leukemia. The main mechanism of DNR is well-established, involving the induction of DNA damage, inhibition of cancer cell proliferation, and stimulation of cell cycle arrest and apoptosis [1]. Although anthracyclines have played a significant role in improving overall survival rates and are considered the most effective cytostatic drugs for treating various types of cancer, the cardiovascular toxicity it induces should not be overlooked.

Even with limited cumulative doses, the incidence of cardiac toxicity in pediatric leukemia patients treated with anthracyclines is still approximately 8.2 %–21 % according to different follow-up times and definitions of varying levels of cardiac toxicity [2–4]. This places a tremendous disease burden on the long-term survival of these patients, particularly in pediatric patients who experience longer lifespans and earlier onset of cardiovascular complications. Large retrospective cohort studies have highlighted cardiovascular disease as the second most prominent factor threatening the long-term survival of these individuals [5].

Besides causing damage to myocardial cells, dysfunction of cardiovascular endothelial cells also plays a substantial role in the development of cardiac toxicity [6,7]. Hence, the restoration of vascular endothelial cells has become a potential target for preventing and treating long-term cardiac toxicity caused by DNR. Extracellular vesicles (EVs) derived from mesenchymal stem cells (MSC-EVs) have demonstrated tremendous potential in tissue regeneration and injury repair. This potential has been observed in numerous animal disease models and clinical trials, for example, reducing myocardial infarct size and limiting ventricular remodel [8,9], attenuating radiation-induced lung vascular damage [10], etc. However, there is currently a lack of clear understanding regarding the potential therapeutic effects and mechanisms of MSC-EVs on vascular injury resulting from DNR. Here, we investigated the effect of MSC-EVs on DNR-damaged human cardiac microvascular endothelial cells (HCMEC) in vitro and developing blood vessels of Chicken Chorioallantoic Membrane (CAM) in vivo.

2. Materials and methods

2.1. Cell acquisition and culture

HuMSCs were grown in α-MEM supplemented with 10 % EVs-free FBS and 1 % penicillin-streptomycin. Immortalized human cardiac microvascular endothelial cell line (HCMEC) was gifted by Dr. Wang Rong (Qilu Hospital, China) and was cultured in ECM (ScienCell, USA). The cells were cultured at 37 °C, 5 % CO_2. CD31-PE (303106), CD34-PE (343606), CD105-PE (32320) and CD309-Alexa Fluor 647 (359910, Biolegend, USA) were used to characterize HCMEC by Flow cytometry (Guava easyCyte 6HT, Millipore, USA).

2.2. Collection and identification of EVs derived from HuMSCs

The conditioned medium of pre-confluent HuMSCs was processed for isolating EVs as previously reported [11]. The identification of isolated EVs was conducted by transmission electron microscopy (TEM, JEM-1200EX, Japan) and Nanoparticle Tracking Analyzer (NTA, Zetaview, Germany), and the protein concentration was quantified using the Micro BCA protein analysis kit (Boster, China). The expression of characteristic proteins CD9 (1:1000; 13174, CST, USA), CD81 (1:1000; 52892, CST), and Calnexin (1:1000; 2433S, CST) were detected by Western blot.

2.3. DNR-induced HCMEC injury model

Cell Counting Kit-8 (CCK8; NCM, China) was used to determine the intervention dosage of DNR (D122335, Aladdin, China) to HCMEC. The IC50 was fitted by GraphPad Prism 8.0.2 (GraphPad Software, USA). Finally, half of IC50 (150 nM) is adopted as the DNR intervention concentration.

2.4. Senescence-associated β-galactosidase (SA-β-Gal) staining

Each group of cells was fixed with β-Gal fixative solution and incubated with the staining working solution (G1580; Solarbio; China). The stained cells were analyzed by Image J (NIH, USA).

2.5. EVs intervention and endocytosis

The dosage of EVs treated to HCMEC was standardized by protein concentration, and two EVs-treated concentration groups (50 μg/mL, 100 μg/mL) were set up.

EVs were labeled with the PKH26 Red Fluorescent Cell Linker Kit and incubated with DNR stimulated-HCMEC for 12 h and observed by laser scanning confocal microscopy (Olympus, Japan).

2.6. Scratch Wound Assay

Cell migration was measured by Scratch Wound Assay. The migration of the cells was quantified by measuring the scratched area covered by the cells using Image J.

2.7. EdU proliferation assay

Cell proliferation was measured using an EdU Cell Proliferation Kit with Alexa Fluor 488 (Epizyme Biotech, China). Cell proliferation was photographed and analyzed by Image J.

2.8. Tube formation assay

HCMEC was seeded in 96-well plated by 50 μL of 1:1 ECM basal medium diluted Growth Factor Reduced-Matrigel (354230, Corning, USA) at a density of 20,000 cells/well in 100 μL/well ECM with or without EVs. Images were taken after 6 h and processed with Image J.

2.9. Transcriptome sequencing and analysis

HCMEC from Blank, DNR, and DNR+EVs groups were collected in duplicate for RNA extraction and sequenced. Differentially expressed genes (DEGs) were screened using DESeq2, with fold change ≥ 1 and adjusted $P < 0.05$ as criteria. All RNA sequencing samples were commissioned and analyzed by Xiuyue Biol (China).

TargetScan (http://www.targetscan.org/), miRDB (https://mirdb.org/), starbase (https://starbase.sysu.edu.cn/) and RNAinter (https://ngdc.cncb.ac.cn/databasecommons/database/id/7218) were applied to predict the target genes of miRNAs.

2.10. RNA interference

HCMEC were transfected with siRNA targeting PARP9 or miR-186-5p mimics (GenePharma, China) using Lipofectamine® 2000 (Invitrogen, USA) according to the manufacturer's instructions. The sequences of the siRNAs and mimics were as Supplementary Material.

2.11. RNA extraction and RT-PCR

Total RNA was extracted using the RNAfast200 RNA Extraction Kit (Fastagen, China), and cDNA was synthesized employing SureScript™ First-Strand cDNA Synthesis Kit (GeneCopoeia, USA). RT-PCR was performed using BlazeTaq™ SYBR® Green qPCR Kit (GeneCopoeia) on the Real-Time Thermocycler (Analytik Jena AG, qTOWER3G, Germany), and gene expression was normalized to the GAPDH. The primer sequences used in this study are listed in Supplementary Material.

2.12. miRNA extraction and RT-PCR

Total miRNA was extracted using the miRcute miRNA Isolation Kit (TIANGEN, China), and cDNA was synthesized employing miRcute Plus miRNA First-Strand cDNA Kit (TIANGEN). RT-PCR was performed using miRcute Plus miRNA SYBR Green qPCR Kit with specific forward primer (CD201-0080, TIANGEN) and the universal reverse primer. Gene expression was normalized to the U6 gene.

2.13. Western blot (WB)

The following antibodies were used: GAPDH (1:5000; 5174S, CST, USA), PARP9 (1:250; ab53796 Abcam, USA), total STAT1 (1:1000, A19563, Abclonal, China), Phospho-STAT1-Y701 (1:1000, AP0054, Abclonal) and horseradish peroxidase-conjugated goat anti-rabbit secondary antibody (1:5000, AB0101, Abways). The relative densitometric analysis was conducted using the Image J.

2.14. CAM assay

The in vivo evaluation of MSC-EVs and miR-186-5p mimics' effect was conducted through the CAM assay. Fertilized eggs were obtained from Shandong Experimental Breeder Farm of No Specific Pathogenic Chicken (Jinan, China) and acclimatized for 9 days in a standard egg incubator at 37 °C and 60 %–70 % relative humidity. Prior to the experiment, DNR (3 nmol/egg), EVs (150 μg/egg), and miR-186-5p mimics (30 pmol/egg) were pre-embedded in 2.5 % agar (Biowest, Spain). On the sixth day of incubation, a circular window with a 1 cm diameter was opened on the eggshell aseptically. The window was then treated with DNR for 24 h, followed by treatment with EVs or miR-186-5p mimics for 48 h. On the ninth day, the CAM was fully exposed and photographed. Each test sample was performed using three eggs. The area of blood vessels was measured using the Image J.

2.15. Statistical analysis

GraphPad Prism 8.0.2 was used for statistical analysis. The quantitative data were examined by normal distribution test and expressed as the mean ± standard error, followed by variance homogeneity test. Two groups of independent samples were compared using unpaired *t*-test. One-way ANOVA and Two-way ANOVA were conducted to determine statistically significant differences among multiple homogeneous groups. For significant ANOVA results, Turkey's multiple comparison test and Dunnett's multiple comparison tests were performed to analyze the differences between controlled groups and multiple homogeneous groups. Results with *P* values less than 0.05 were considered significant.

3. Results

3.1. Identification of MSC-EVs

MSC-EVs were extracted and identified by TEM (Fig. 1A), WB (Fig. 1B) and NTA (Fig. 1C). These findings confirm the successful isolation of MSC-EVs.

3.2. Establishment of DNR-damaged HCMEC models

Typical markers of HCMEC were identified by flow cytometry (Fig. 1D). CCK-8 assay was used to explore the appropriate intervention dosage of DNR to HCMEC (Fig. 1E). DNR-damaged HCMEC showed high activity of SA-β-Gal, which indicated cellular senescence (Fig. 1F). The experimental design flowchart can be seen in Fig. 1G. PKH-26-labeled MSC-EVs were incubated with DNR-damaged HCMEC, and the data showed MSC-EVs were efficiently internalized (Fig. 1H).

3.3. MSC-EVs rehabilitated cellular function and alleviated senescence of DNR-damaged HCMEC

Scratch wound assays, EdU assays, tube formation assays, and SA-β-Gal staining indicated that MSC-EVs significantly improved the migration (Fig. 2A and B), proliferation (Fig. 2C and D), and angiogenesis capacity (Fig. 2E and F), meanwhile alleviating cell senescence (Fig. 2G and H) of DNR-damaged HCMEC.

3.4. MSC-EVs reduced expression of inflammatory adhesion molecule ICAM-1 and growth inhibition molecule VE-cadherin of DNR-damaged HCMEC

ICAM-1 is a cell surface glycoprotein expressed at a low basal level in endothelial cells, but is up-regulated in response to inflammatory stimulation and other injury [12]. RT-PCR results indicated that MSC-EVs downregulated the mRNA expression of ICAM-1 (Fig. 2I). VE-cadherin is an adhesion molecule of endothelial cells, which can interact and co-cluster with growth factor receptors and limit their intracellular signals, thus inhibiting the growth and motility of endothelial cells [13]. Our result showed MSC-EVs might relieve the growth inhibition of DNR-damaged HCMEC by downregulating VE-cadherin mRNA expression (Fig. 2J).

3.5. MSC-EVs improved angiogenesis in the DNR-damaged CAM model

To validate the reparative effect of MSC-EVs on DNR-damaged blood vessels in vivo, we conducted a CAM assay. Based on the results of the concentration titration of MSC-EVs, we have selected 150 μg/egg as the final intervention concentration (Sup Fig. 1A and B). The results demonstrated that MSC-EVs significantly promoted the angiogenesis in the CAM damaged by DNR (Fig. 2K and L).

3.6. MSC-EVs inhibited the activation of the type I interferon (IFN-I) signal pathway in DNR-damaged HCMEC

We conducted transcriptomic sequencing on HCMEC samples from the control group, DNR group, and DNR+MSC-EVs group (Fig. 3A), and specifically screened for genes that were upregulated in the DNR group compared to the Blank group, meanwhile were downregulated in the DNR+MSC-EVs group compared to the DNR group and vice versa (Fig. 3B). The heatmap displayed the differentially expressed genes (Fig. 3C). GO and GSEA enrichment analysis indicated that the IFN-I and STAT pathways were particularly notable (Fig. 3D and E). Heatmap showed that MSC-EVs inhibited

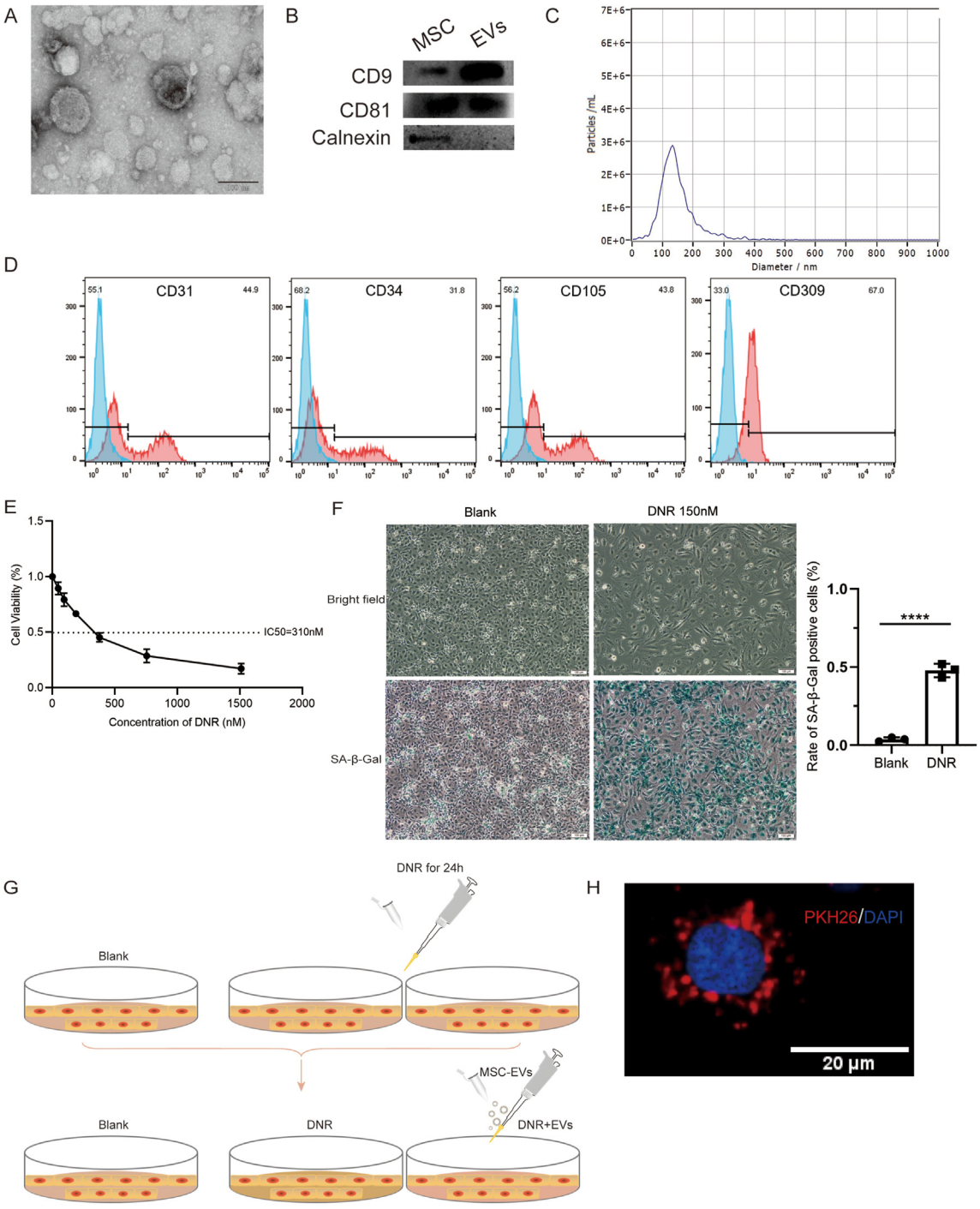

Fig. 1. MSC-EVs could be internalized by daunorubicin (DNR)-damaged HCMEC **A**. Ultrastructure of EVs observed by transmission electron microscopy **B**. Western blotting of the EVs markers CD9, CD81 and calnexin in lysates from MSC and MSC-EVs **C**. The average particle size distribution of MSC-EVs **D**. Immunophenotypes of HCMEC as determined by flow cytometry **E**. The effects of different doses of DNR for the cell viability of HCMEC, and half of IC50 was used for further experiments **F**. Morphological changes and SA-β-Gal positive ratio of HCMEC under DNR intervention. Data are presented as the mean ± SD of three replicates. ****$P < 0.0001$ **G**. The flow chart of the experimental design. HCMEC were subjected to DNR for 24 h when confluency reached 80 %. Afterward, the culture medium was replaced with or without MSC-EVs for the corresponding time **H**. PKH 26-labeled MSC-EVs (red) were internalized by DNR-damaged HCMEC.

the expression of IFN-I signaling pathway-related molecules in DNR-damaged HCMEC (Fig. 3F).

3.7. miR-186-5p enriched in MSC-EVs downregulated the expression of PARP9

As STAT1 acts as the canonical signal molecule in the IFN-I pathway and could inhibit cell growth, and induce cell cycle arrest and cellular senescence [14–16], we screened potential target genes that may interact with STAT1, and poly (ADP-ribose) polymerase family member 9 (PARP9) has garnered our attention. PARP9 and the family to which it belongs participate in various cellular processes such as DNA repair, genomic stability, and programmed cell death [17]. It has been proved that PARP9 promotes phosphorylation of STAT1 in macrophages. The network-based analysis indicates that PARP9 has a potential impact on the

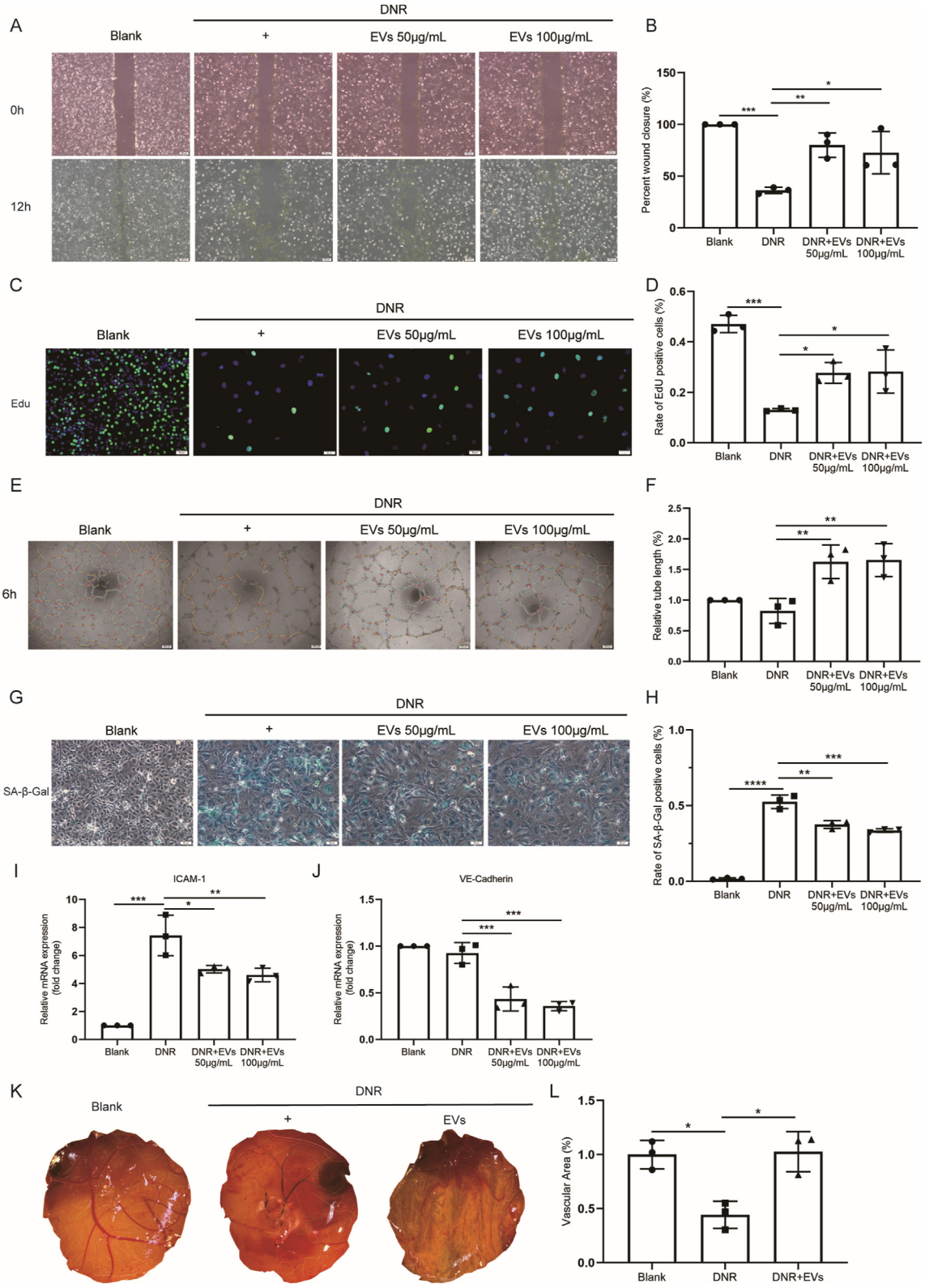

Fig. 2. MSC-EVs restore the cellular function and alleviate senescence of DNR-damaged HCMEC **A, B**. Scratch wound Assay indicates the effects of MSC-EVs on cell migration of DNR-damaged HCMEC. Scale bar represents 100 μm **C, D.** Edu Proliferation Assay shows that MSC-EVs improve cell proliferation of DNR-damaged HCMEC. Scale bar represents 50 μm **E, F**. Tube formation assay demonstrates the effects of MSC-EVs on angiogenesis of DNR-damaged HCMEC. Scale bar represents 200 μm **G, H.** SA-β-Gal staining suggests that MSC-EVs alleviate cellular senescence of DNR-damaged HCMEC. Scale bar represents 50 μm **I, J.** The mRNA level of ICAM-1 and VE-cadherin in DNR-damaged HCMEC. **K, L**. Chicken Chorioallantoic Membrane (CAM) assay demonstrates the effects of MSC-EVs on angiogenesis of DNR-damaged CAM. Data are presented as the mean ± SD of three replicates. $*P < 0.05$, $**P < 0.01$, $***P < 0.001$, $****P < 0.0001$.

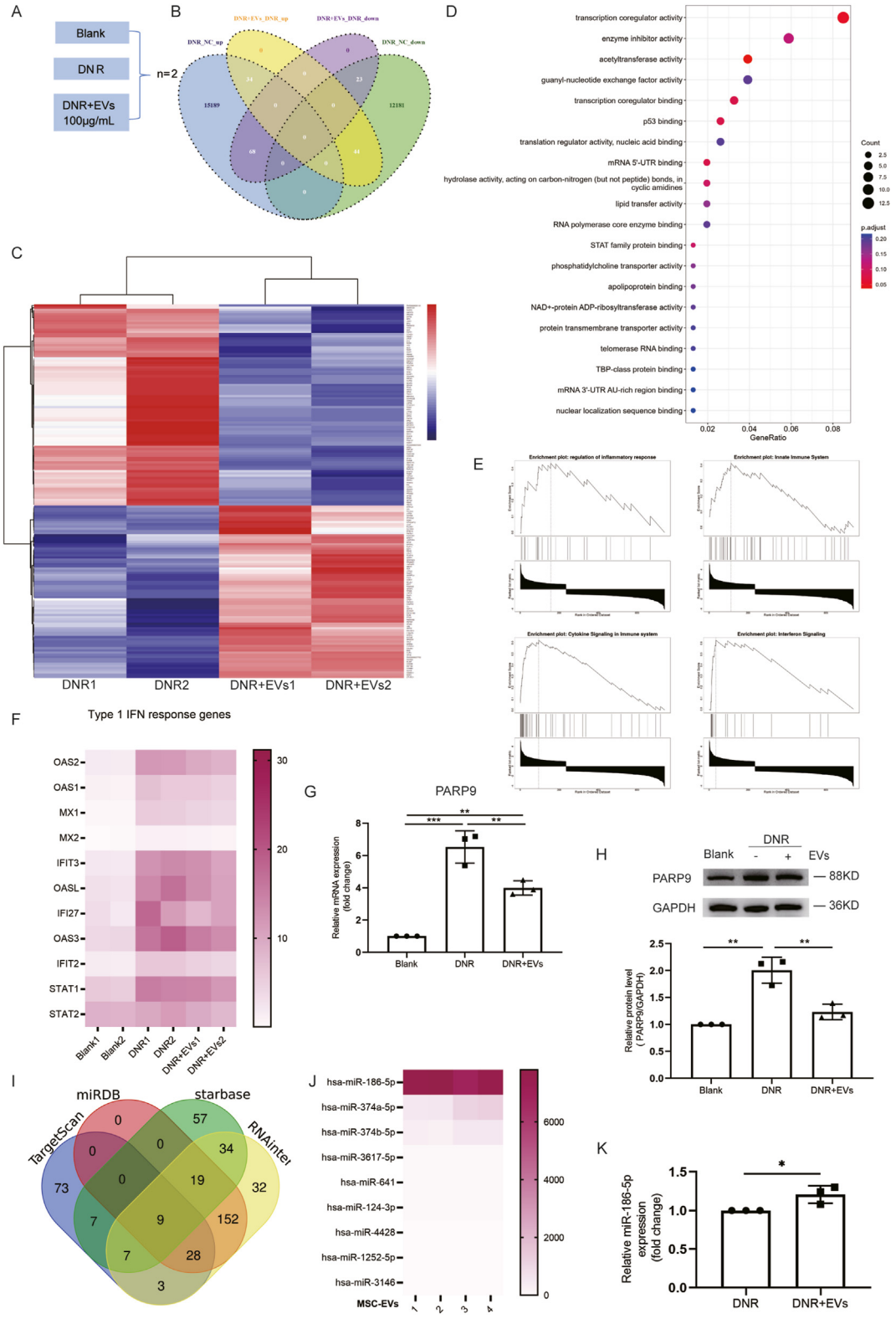

Fig. 3. Transcriptome sequencing and bioinformatics tools screen out the miR-186-5p-PARP9 axis **A, B**. Transcriptome samples and screening rules **C, D.** Heat map and GO enrichment analysis bubble map of differential genes **E.** GSEA enrichment analysis suggests that MSC-EVs down-regulate the type 1 interferon (IFN-I) signaling pathway in DNR-damaged HCMEC **F**. Heatmap of the representative genes in IFN-I pathway **G, H**. Effects of MSC-EVs on PARP9 expression were determined by RT-PCR and WB **I.** Venn diagram of 9 miRNAs targeting PARP9 by prediction tools **J**. The GSE211008 dataset suggests that miR-186-5p has the highest expression level among 9 predicted miRNAs in MSC-EVs **K**. Effects of MSC-EVs on miR-186-5p expression were determined by RT-PCR. Data are presented as the mean ± SD of three replicates. $^{*}P < 0.05$, $^{**}P < 0.01$, $^{***}P < 0.001$.

pathogenesis of arterial disease [18]. We validated the results of transcriptome sequencing with RT-PCR (Fig. 3G) and WB (Fig. 3H), and confirmed that PARP9 was upregulated in DNR-damaged HCMEC while MSC-EVs partly suppressed this upregulation effect.

We employed bioinformatics tools to predict the upstream regulatory molecules of PARP9. We performed an intersection analysis between the highly expressed miRNAs in MSC-EVs from publicly available datasets (GSE211008) and the results obtained from predictive software (Fig. 3I and J). Among the predicted miRNAs, miR-186-5p exhibited the highest abundance in MSC-EVs. Taking into account both the algorithmic predictions and the empirical results, we ultimately identified miR-186-5p as a potential target of PARP9, which had been validated through dual-luciferase reporter assay [19]. RT-PCR demonstrated that MSC-EVs intervention upregulated miR-186-5p expression compared to the DNR-damaged group (Fig. 3K). These combined results provide compelling evidence supporting the involvement of miR-186-5p as a key player in the regulatory network associated with PARP9.

3.8. PARP9 silencing improved the migration, proliferation and attenuated cellular senescence of DNR-damaged HCMEC by inhibiting the STAT1/pSTAT1 pathway

To elucidate the role of PARP9 in the functional restoration of DNR-damaged HCMEC, we conducted RNA interference targeting PARP9 (Sup Fig. 1C–F). The cell functional assays indicated that knocking down PARP9 significantly improved the migration (Fig. 4A and B) and proliferation (Fig. 4C and D), meanwhile alleviating cell senescence (Fig. 4E and F) of DNR-damaged HCMEC. The

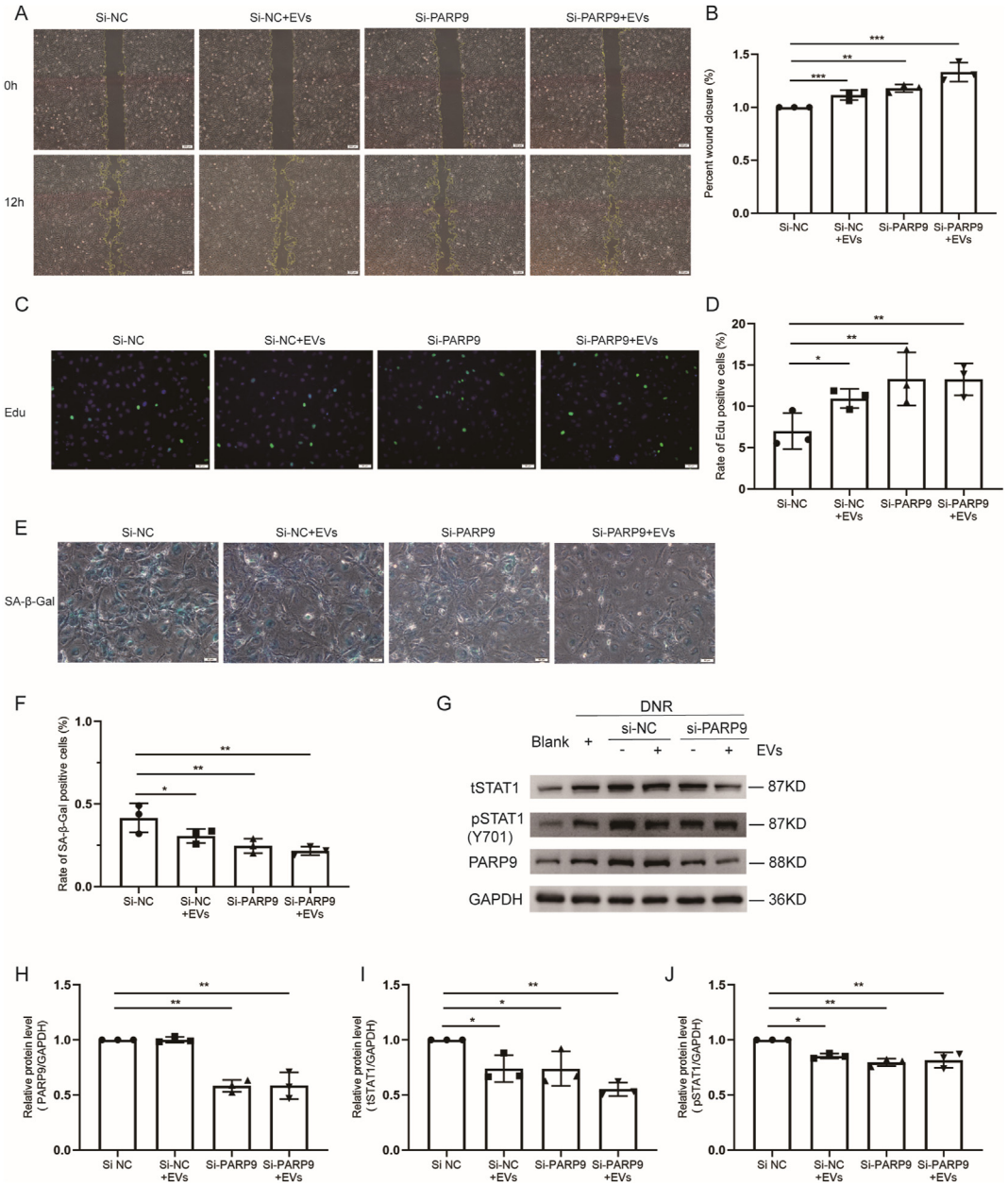

Fig. 4. MSC-EVs downregulated PARP9 to restore the cellular function and alleviate senescence of DNR-damaged HCMEC PARP9 silencing improved the migration (**A, B**), proliferation (**C, D**) and attenuated cellular senescence (**E, F**) of DNR-damaged HCMEC **G-J**. The relative protein level of PARP9, STAT1 and pSTAT1 in si-PARP9 DNR-damaged HCMEC with or without MSC-EVs. Data are presented as the mean ± SD of three replicates. $*P < 0.05$, $**P < 0.01$, $***P < 0.001$.

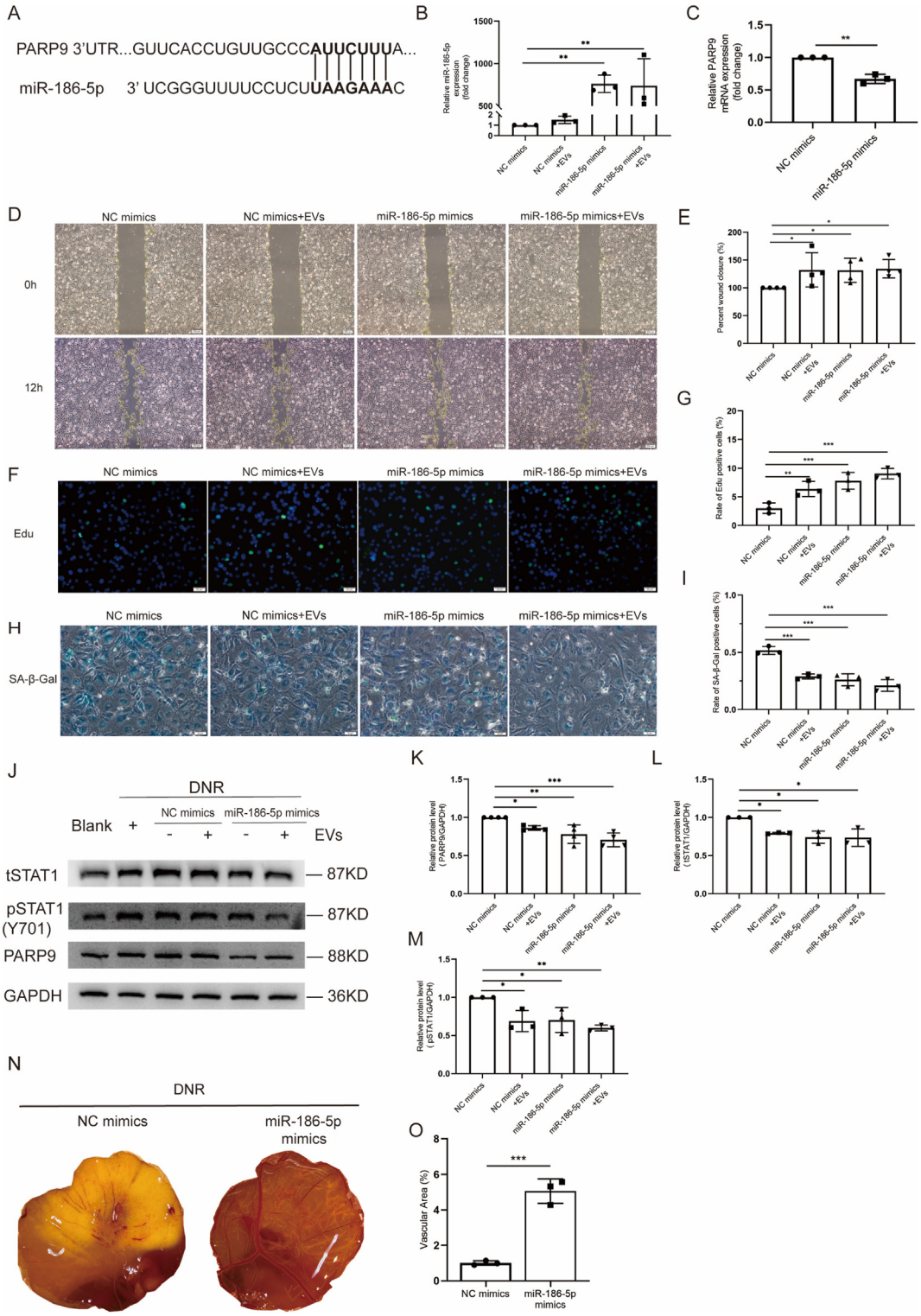

Fig. 5. MSC-EVs disrupted the PARP9-STAT1/pSTAT1 signaling pathway by delivering miR-186-5p **A**. The binding site of miR-186-5p with 3′ UTR region of PARP9 **B**. The transfection efficiency of miR-186-5p mimics examined by RT-PCR in DNR-damaged HCMEC **C**. The mRNA expression level of the target gene PARP9 was downregulated by miR-186-5p mimics. miR-186-5p mimics improved the migration (**D, E**), proliferation (**F, G**) and attenuated cellular senescence (**H, I**) of DNR-damaged HCMEC. **J-M**. miR-186-5p mimics downregulated the protein expression level of PARP9, STAT1 and pSTAT1 in DNR-damaged HCMEC with or without MSC-EVs. **N, O.** miR-186-5p mimics improved the angiogenesis of DNR-damaged CAM. Data are presented as the mean ± SD of three replicates. *P < 0.05, **P < 0.01, ***P < 0.001.

downregulation of PARP9 expression also inhibited the expression of total STAT1 and phosphorylated STAT1 (Fig. 4G–J).

3.9. miR-186-5p improved the migration, proliferation and attenuated cellular senescence of DNR-damaged HCMEC by PARP9-STAT1/pSTAT1 axis

To investigate the upstream mechanism of how miRNA derived from MSC-EVs regulates the expression of PARP9, we transfected DNR-damaged HCMEC cells with miR-186-5p mimics. The binding site of miR-186-5p with 3' UTR region of PARP9 was illustrated in Fig. 5A. RT-PCR verified that the expression of miR-186-5p was increased in the transfected cells, and at the same time, the expression of the target gene PARP9 was downregulated (Fig. 5B and C). Cell function assays demonstrated that miR-186-5p mimics significantly ameliorated the migration (Fig. 5D and E) and proliferation (Fig. 5F and G) and also mitigated cell senescence (Fig. 5H and I) of DNR-damaged HCMEC. Consistently, the downregulation of PARP9 expression mediated by miR-186-5p mimics inhibits the expression of STAT1/pSTAT1 at protein levels (Fig. 5J-M). In vivo experiments also confirmed that miR-186-5p mimics significantly improved angiogenesis in the DNR-damaged CAM (Fig. 5N and O).

In summary, our results indicate that the miR-186-5p-PARP9-STAT1/pSTAT1 axis plays a crucial role in mediating the functional reconstruction and attenuation of cellular senescence in DNR-damaged HCMEC cells by MSC-EVs (Graphical abstract, by Figdraw).

4. Discussion

Cardiovascular disease has emerged as a significant cause of premature morbidity and mortality among childhood cancer survivors. Previous research has focused on understanding the mechanisms of cardiac toxicity induced by anthracyclines initiated with the direct damage to myocytes [20]. However, vascular damage also plays a critical role in the pathophysiology. Huang C. et al. indicate that vascular dysfunction may be the primary factor contributing to cardiac toxicity, particularly in terms of long-term effects [7]. Besides, a recent study suggested that perivascular fibrosis occurs even earlier than damage to myocytes [6,21]. Here, we successfully simulated the detrimental effects of DNR on HCMEC and developing vessels of CAM, which included inhibiting cell function, inducing cellular senescence, and hindering the development of blood vessels in vivo.

Several therapeutic measures have been developed to prevent or alleviate the cardiotoxicity of anthracycline drugs. These include cardioprotective agents such as dexrazoxane, the only FDA-approved drug for treating anthracycline-induced cardiotoxicity, which could reduce ROS production [22,23]. However, there are currently no effective long-term preventive or treatment measures for cardiovascular complications. Cells and their derivatives are new promising therapeutic options. Studies have shown that MSCs and their derived EVs can repair myocardial damage through multiple mechanisms, such as modulating ER stress-induced apoptosis [24], and attenuating cellular senescence [25], etc. Endothelial cells are also targets for compounds. Himangshu Sonowal et al. demonstrated that fidarestat, an aldose reductase inhibitor, prevented ROS accumulation and caspase-3 activation in anthracycline-stressed HUVECs [26]. Prior research findings also substantiated the capability of MSC-EVs to mitigate cellular senescence, and promote cell proliferation in HUVEC, specifically under conditions of oxidative stress-induced senescence [27]. Our study provides new evidence of considerable reparative effects that MSC-EVs could act as a new therapeutic option for DNR-damaged endothelial cells and developing blood vessels. Regarding the clinical applications of MSC-EVs for vascular injury repair, there is currently no reported clinical trial that delineates the specific administration methods and dosages. However, several articles have documented the details of MSC-EV administration in animal experiments. For example, Lei et al. used a dosage of 100 μg/kg to treat radiation-induced lung vascular damage in mice [10]. Xiao et al. demonstrated that a dosage of 200 μg/mice of MSC-EVs promoted angiogenesis in diabetic wounds [27]. In our in vitro experiments, we used a concentration range commonly reported as therapeutically relevant, indicating potential clinical applicability. Nonetheless, further investigations, including in vivo studies and dose-response assessments, are necessary to determine the optimal concentration for clinical administration.

Our RNA sequencing analysis uncovered that MSC-EVs exert a down regulatory effect on the IFN-I signaling pathway in DNR-damaged HCMEC. This pathway is known to be induced by the Cyclic GMP-AMP Synthase (cGAS) and Stimulator of Interferon Genes (STING) pathway in response to damaged double-stranded DNA breaks, subsequently activating the p53 pathway, and facilitating cellular senescence [28]. Studies demonstrated the significant involvement of the IFN-I pathway in both aging and degenerative diseases. IFN-I-dependent gene expression profiles have been identified in multiple aging organs and tissues. Interfering with IFN-I signaling or the key signaling molecule within this pathway, phosphorylated STAT1, has shown partial restoration of cognitive function and hippocampal neurogenesis [29], alleviating inflammation infiltration in the aged lung [30]. Based on our findings and previous well-established research, inhibiting the IFN-1 pathway may serve as an effective approach for preventing or reversing vascular senescence caused by DNR.

Integrating miRNA sequencing data of MSC-EVs from public databases with our RNA sequencing data allowed us uncovering the miR-186-5p-PAPR9-STAT1/pSTAT1 axis. The members of PARP family are named due to the conserved catalytic domain, which allows them to transfer the ADP-ribose moieties from NAD to protein acceptors and recruit DNA repair proteins to the damage sites [31]. The specific function of PARP9 has not been fully elucidated to date. Our findings elucidate that inhibition of PARP9 by miR-186-5p downregulates the expression of STAT1/pSTAT1 at the protein level. Consistently, silencing of PARP9 reduces the phosphorylation of STAT1 in human macrophages treated with IFN γ, which suggests that PARP9 may activate the IFNγ-STAT1 pathway and induce proinflammatory activation [18]. Conversely, evidence also suggests that PARP9 enhances the phosphorylation of both STAT1α and STAT1β, facilitating their nuclear translocation. This promotes antagonistic effects and the nuclear accumulation of the transcriptional repressive isoform, STAT1β. Consequently, PARP9 exerts an inhibitory role against the anti-proliferative and pro-apoptotic IFNγ-STAT1-IRF1-p53 axis, thus promotes proliferation in diffuse large B-cell lymphoma [32]. Our study enhanced the evidence that PARP9 exerted a positive regulatory role in the STAT1 signaling pathway. However, the specific molecular mechanisms through which PARP9 positively regulates STAT1 phosphorylation remain elusive. Future investigations are warranted to unravel and comprehend these intricate mechanisms.

5. Conclusions

In short, our findings show that miR-186-5p-enriched MSC-EVs can effectively restore the cellular function of DNR-damaged HCMEC by downregulating PARP9 expression and subsequently inhibiting the STAT1/pSTAT1 pathway. The pro-angiogenesis effect was validated on the developing vessels through the in vivo CAM assay. This suggests that MSC-EVs could serve as a potential therapeutic approach for treating vascular injuries caused by anthracyclines.

Ethics approval

Not applicable.

Consent for publication

Not applicable.

Availability of data and materials

The datasets presented for this study can be found in NCBI online repositories: GSE240194.

Funding

This work was supported by the Natural Science Foundation of Shandong Province [No. ZR2023MH079]; Ji Nan Science and Technology Bureau [No. JNKCJN202201]; and Shandong Province Enterprise Innovation Ability Enhancement Project [No. 2022TSGC2001].

Authors' contributions

Shule Zhang: Validation, Investigation, Data curation, Formal analysis, Writing original draft. Dong Li: Resources, Data curation, Formal analysis, Writing-review & editing. Linghong Liu: Validation, Investigation, Data curation, Formal analysis. Qing Shi: Resources, Data curation, Formal analysis. Xiuli Ju: Methodology, Writing-review & editing, Supervision, Project administration, Funding acquisition.

Declaration of Generative AI and AI-assisted technologies in the writing process

During the writing process, we did not use generative AI or AI-assisted technology.

Declaration of competing interest

The authors declare that they have no known competing financial interests or personal relationships that could have appeared to influence the work reported in this paper.

Acknowledgments

We are grateful to Dr. Wang for providing the HCMEC immortalized cell line, and Dr. Liu, for valuable discussions on RNA sequencing and analysis. We also thank Translational Medicine Core Facility of Shandong University for consultation and instrument availability that supported this work.

Appendix A. Supplementary data

Supplementary data to this article can be found online at https://doi.org/10.1016/j.reth.2024.01.011.

References

[1] Henriksen PA. Anthracycline cardiotoxicity: an update on mechanisms, monitoring and prevention. Heart 2018;104:971–7.
[2] Getz KD, Sung L, Ky B, Gerbing RB, Leger KJ, Leahy AB, Sack L, Woods WG, Alonzo T, Gamis A, Aplenc R. Occurrence of treatment-related cardiotoxicity and its impact on outcomes among children treated in the AAML0531 clinical trial: a report from the children's oncology group. J Clin Oncol 2019;37:12–21.
[3] Boluda B, Solana-Altabella A, Cano I, Martínez-Cuadrón D, Acuña-Cruz E, Torres-Miñana L, Rodríguez-Veiga R, Navarro-Vicente I, Martínez-Campuzano D, García-Ruiz R, Lloret P, Asensi P, Osa-Sáez A, Aguero J, Rodríguez-Serrano M, Buendía-Fuentes F, Megías-Vericat JE, Martín-Herreros B, Barragán E, Sargas C, Salas M, Wooddell M, Dharmani C, Sanz MA, De la Rubia J, Montesinos P. Incidence and risk factors for development of cardiac toxicity in adult patients with newly diagnosed acute myeloid leukemia. Cancers 2023;15.
[4] Lipshultz SE, Adams MJ, Colan SD, Constine LS, Herman EH, Hsu DT, Hudson MM, Kremer LC, Landy DC, Miller TL, Oeffinger KC, Rosenthal DN, Sable CA, Sallan SE, Singh GK, Steinberger J, Cochran TR, Wilkinson JD. Long-term cardiovascular toxicity in children, adolescents, and young adults who receive cancer therapy: pathophysiology, course, monitoring, management, prevention, and research directions: a scientific statement from the American Heart Association. Circulation 2013;128:1927–95.
[5] Dixon SB, Liu Q, Chow EJ, Oeffinger KC, Nathan PC, Howell RM, Leisenring WM, Ehrhardt MJ, Ness KK, Krull KR, Mertens AC, Hudson MM, Robison LL, Yasui Y, Armstrong GT. Specific causes of excess late mortality and association with modifiable risk factors among survivors of childhood cancer: a report from the Childhood Cancer Survivor Study cohort. Lancet 2023;401:1447–57.
[6] Pan J-a, Zhang H, Lin H, Gao L, Zhang H-l, Zhang J-f, Wang C-q, Gu J. Irisin ameliorates doxorubicin-induced cardiac perivascular fibrosis through inhibiting endothelial-to-mesenchymal transition by regulating ROS accumulation and autophagy disorder in endothelial cells. Redox Biol 2021;46:102120.
[7] Huang C, Zhang X, Ramil JM, Rikka S, Kim L, Lee Y, Gude NA, Thistlethwaite PA, Sussman MA, Gottlieb RA, Gustafsson AB. Juvenile exposure to anthracyclines impairs cardiac progenitor cell function and vascularization resulting in greater susceptibility to stress-induced myocardial injury in adult mice. Circulation 2010;121:675–83.
[8] Timmers L, Lim SK, Arslan F, Armstrong JS, Hoefer IE, Doevendans PA, Piek JJ, El Oakley RM, Choo A, Lee CN, Pasterkamp G, de Kleijn DP. Reduction of myocardial infarct size by human mesenchymal stem cell conditioned medium. Stem Cell Res 2007;1:129–37.
[9] Monguió-Tortajada M, Prat-Vidal C, Martínez-Falguera D, Teis A, Soler-Botija C, Courageux Y, Munizaga-Larroudé M, Moron-Font M, Bayes-Genis A, Borràs FE, Roura S, Gálvez-Montón C. Acellular cardiac scaffolds enriched with MSC-derived extracellular vesicles limit ventricular remodelling and exert local and systemic immunomodulation in a myocardial infarction porcine model. Theranostics 2022;12:4656–70.
[10] Lei X, He N, Zhu L, Zhou M, Zhang K, Wang C, Huang H, Chen S, Li Y, Liu Q, Han Z, Guo Z, Han Z, Li Z. Mesenchymal stem cell-derived extracellular vesicles attenuate radiation-induced lung injury via miRNA-214-3p. Antioxidants Redox Signal 2021;35:849–62.
[11] Théry C, Amigorena S, Raposo G, Clayton A. Isolation and Characterization of Exosomes from Cell Culture Supernatants and Biological Fluids. Current Protocols in Cell Biology 2006;30:3.22.1–3.22.29.
[12] Bui TM, Wiesolek HL, Sumagin R. ICAM-1: a master regulator of cellular responses in inflammation, injury resolution, and tumorigenesis. J Leukoc Biol 2020;108:787–99.
[13] Giannotta M, Trani M, Dejana E. VE-cadherin and endothelial adherens junctions: active guardians of vascular integrity. Dev Cell 2013;26:441–54.
[14] Ivashkiv LB, Donlin LT. Regulation of type I interferon responses. Nat Rev Immunol 2014;14:36–49.
[15] Hu X, Li J, Fu M, Zhao X, Wang W. The JAK/STAT signaling pathway: from bench to clinic. Signal Transduct Targeted Ther 2021;6:402.
[16] Zhang Y, Yang Y, Yang F, Liu X, Zhan P, Wu J, Wang X, Wang Z, Tang W, Sun Y, Zhang Y, Xu Q, Shang J, Zhen J, Liu M, Yi F. HDAC9-mediated epithelial cell cycle arrest in G2/M contributes to kidney fibrosis in male mice. Nat Commun 2023;14:3007.
[17] Lüscher B, Ahel I, Altmeyer M, Ashworth A, Bai P, Chang P, Cohen M, Corda D, Dantzer F, Daugherty MD, Dawson TM, Dawson VL, Deindl S, Fehr AR, Feijs KLH, Filippov DV, Gagné JP, Grimaldi G, Guettler S, Hoch NC, Hottiger MO, Korn P, Kraus WL, Ladurner A, Lehtiö L, Leung AKL, Lord CJ, Mangerich A, Matic I, Matthews J, Moldovan GL, Moss J, Natoli G, Nielsen ML, Niepel M, Nolte F, Pascal J, Paschal BM, Pawłowski K, Poirier GG, Smith S, Timinszky G, Wang ZQ, Yélamos J, Yu X, Zaja R, Ziegler M. ADP-ribosyltransferases, an update on function and nomenclature. FEBS J 2022;289:7399–410.
[18] Iwata H, Goettsch C, Sharma A, Ricchiuto P, Goh WW, Halu A, Yamada I, Yoshida H, Hara T, Wei M, Inoue N, Fukuda D, Mojcher A, Mattson PC, Barabási AL, Boothby M, Aikawa E, Singh SA, Aikawa M. PARP9 and PARP14 cross-regulate macrophage activation via STAT1 ADP-ribosylation. Nat Commun 2016;7:12849.
[19] Ma Y, Zhang D, Wu H, Li P, Zhao W, Yang X, Xing X, Li S, Li J. Circular RNA PRKCI silencing represses esophageal cancer progression and elevates cell radiosensitivity through regulating the miR-186-5p/PARP9 axis. Life Sci 2020;259:118168.
[20] Sobczuk P, Czerwińska M, Kleibert M, Cudnoch-Jędrzejewska A. Anthracycline-induced cardiotoxicity and renin-angiotensin-aldosterone system-from molecular mechanisms to therapeutic applications. Heart Fail Rev 2022;27:295–319.
[21] Tanaka R, Umemura M, Narikawa M, Hikichi M, Osaw K, Fujita T, Yokoyama U, Ishigami T, Tamura K, Ishikawa Y. Reactive fibrosis precedes doxorubicin-induced heart failure through sterile inflammation. ESC Heart Fail 2020;7:588–603.
[22] Jirkovský E, Jirkovská A, Bureš J, Chládek J, Lenčová O, Stariat J, Pokorná Z, Karabanovich G, Roh J, Brázdová P, Šimůnek T, Kovaříková P, Štěrba M. Pharmacokinetics of the cardioprotective drug dexrazoxane and its active metabolite ADR-925 with focus on cardiomyocytes and the heart. J Pharmacol Exp Therapeut 2018;364:433–46.

[23] Lebrecht D, Geist A, Ketelsen UP, Haberstroh J, Setzer B, Walker UA. Dexrazoxane prevents doxorubicin-induced long-term cardiotoxicity and protects myocardial mitochondria from genetic and functional lesions in rats. Br J Pharmacol 2007;151:771–8.
[24] Huang A, Liu Y, Qi X, Chen S, Huang H, Zhang J, Han Z, Han ZC, Li Z. Intravenously transplanted mesenchymal stromal cells: a new endocrine reservoir for cardioprotection. Stem Cell Res Ther 2022;13:253.
[25] Chen L, Xia W, Hou M. Mesenchymal stem cells attenuate doxorubicin-induced cellular senescence through the VEGF/Notch/TGF-β signaling pathway in H9c2 cardiomyocytes. Int J Mol Med 2018;42:674–84.
[26] Sonowal H, Pal P, Shukla K, Saxena A, Srivastava SK, Ramana KV. Aldose reductase inhibitor, fidarestat prevents doxorubicin-induced endothelial cell death and dysfunction. Biochem Pharmacol 2018;150:181–90.
[27] Xiao X, Xu M, Yu H, Wang L, Li X, Rak J, Wang S, Zhao RC. Mesenchymal stem cell-derived small extracellular vesicles mitigate oxidative stress-induced senescence in endothelial cells via regulation of miR-146a/Src. Signal Transduct Targeted Ther 2021;6:354.
[28] Yu Q, Katlinskaya YV, Carbone CJ, Zhao B, Katlinski KV, Zheng H, Guha M, Li N, Chen Q, Yang T, Lengner CJ, Greenberg RA, Johnson FB, Fuchs SY. DNA-damage-induced type I interferon promotes senescence and inhibits stem cell function. Cell Rep 2015;11:785–97.
[29] Baruch K, Deczkowska A, David E, Castellano JM, Miller O, Kertser A, Berkutzki T, Barnett-Itzhaki Z, Bezalel D, Wyss-Coray T, Amit I, Schwartz M. Aging. Aging-induced type I interferon response at the choroid plexus negatively affects brain function. Science 2014;346:89–93.
[30] D'Souza SS, Zhang Y, Bailey JT, Fung ITH, Kuentzel ML, Chittur SV, Yang Q. Type I Interferon signaling controls the accumulation and transcriptomes of monocytes in the aged lung. Aging Cell 2021;20:e13470.
[31] Spiegel JO, Van Houten B, Durrant JD. PARP1: structural insights and pharmacological targets for inhibition. DNA Repair 2021;103:103125.
[32] Camicia R, Bachmann SB, Winkler HC, Beer M, Tinguely M, Haralambieva E, Hassa PO. BAL1/ARTD9 represses the anti-proliferative and pro-apoptotic IFNγ-STAT1-IRF1-p53 axis in diffuse large B-cell lymphoma. J Cell Sci 2013;126:1969–80.